

M. Schäfer¹, R. Keimer² & O. Bertram¹

¹German Aerospace Center (DLR), Institute for Flight Systems, Lilienthalplatz 7, 38108 Braunschweig, Germany

²German Aerospace Center (DLR), Institute for Lightweight Systems, Lilienthalplatz 7, 38108 Braunschweig, Germany

Abstract

Climate-friendly technologies are at the forefront of current research topics. Consequently, the aircraft industry is undergoing significant changes. In addition to disruptive technologies, such as hydrogen propulsion or flyingwing concepts, technologies that reduce fuel consumption are still necessary to maintain the economic operation of aircraft.

One of these technologies is the morphing control surface. Through continuous adaptation of the wing profile, shape-variable control surfaces on the wing have the potential to significantly enhance aerodynamic performance. In addition to the lower fuel consumption, the elimination of gaps on the wing can also reduce noise. To realize such an adaptive profile within the wing, technologies enabling structural deformation are required. The primary challenge in developing such technologies is to ensure both the flexibility for the shape-variable structure and the necessary stiffness. Various technologies are being explored and developed to use the benefits of such shape-variable structures. Both the integration into the wing and the certification of these novel technologies pose essential considerations regarding installation space, weight, and safety aspects.

At the German Aerospace Center, a morphing technology has been developed that allows changing the wing profile. This technology is based on pressure cells actuated by a fluid. To implement this technology in the wing, a suitable system architecture must be developed. In this paper, the design, test environment, and experimental results of an actuation system for this morphing technology are presented. The focus was on demonstrating the functionality of the structural technology in conjunction with the system architecture. For this purpose, various tests were conducted in the areas of system control and dynamic behavior.

Keywords: system design; system architecture; flight control; morphing

1. Introduction

Morphing has played a role in aviation since the pioneering flight of the Wright Brothers. During their initial flight, aircraft control was achieved through the mechanical deformation of the wings. As flying speeds increased and demands for structural integrity heightened, rigid control surfaces became the standard in modern aircraft. Bolonkin et al. [1] were able to show in simulations that aircraft performance can be improved by a variable camber of the wing profile in almost every point of the flight envelope. An adjustment of the camber can be used to reduce the drag coefficient or increase the lift coefficient. This is associated with reduced fuel consumption, resulting in lower operational costs and a diminished environmental impact of aircraft.

In order to realize morphing wing technologies a deformation of the wing structure must be possible. A major challenge in the development of morphing technologies is to enable both the flexibility for the shape-variable structure and to ensure the necessary stiffness [2]. As described in preliminary work in [3], in the classical design approach of control surfaces, there exists a separation between structure and actuation system. For morphing technologies, these two domains are often implemented together to achieve the desired functionality. Various actuation concepts, such as traditional actuators [4], shape memory alloys [5], piezoelectric actuators [6], or cells deformed by a suitable fluid [7], are employed in research. However, in the design phase, the focus is typically on the structure itself, with the actuation system only being marginally discussed. Other critical factors, such as space, safety,

and certification aspects, are frequently neglected. Nevertheless, these considerations are crucial for the application of new functions and technologies in aviation.

Morphing can be implemented in different ways and for different functions. Concepts include variable wingspan, wing morphing or variable wing profiles. This paper discusses the design and testing process of an actuation system for a morphing technology for variable wing profiles, which is based on fluid-pressurized cells. In this process, an integral design of actuation system and structure is conducted early on in the design. Consequently, safety and integration aspects can influence structural design at an early stage. This approach aims to facilitate faster development and integration of new functionalities in aircraft. The focus of this paper lies in activities related to system development. Previous publications have outlined the preliminary design [3], [8]. Based on the results of these preliminary works, a test environment was defined and constructed. Using this setup, experiments were conducted to investigate both the functionality and performance of morphing technology.

Chapter 2 provides an explanation of the functioning principle of the morphing structure. Following, Chapter 3 offers a brief summary of the system design. The main part describes the test environment and presents the experimental results. Finally, a discussion of the results and an outlook on future work are provided in Chapter 5.

2. Morphing Structure

The concept of the morphing control surface used in this work is based on biologically inspired engineering. These so-called Fluid Actuated Morphing Unit Structures (FAMoUS) [2] are inspired by the hydrostatic skeletons of sea anemones. The functional principle of the pressure cells is shown in Figure 1. To implement the concept as a control surface, pressure cells were designed. These cells consist of ring-shaped, rigid structures surrounded by elastic material. Within these cells, there is a cavity filled with a fluid. Applying pressure allows for a directed elongation of the cells, and by combining two such cells, a deflection can be achieved. However, only the first half of the control surface consists of this deformable structure, while the second half remains a traditional rigid trailing edge.

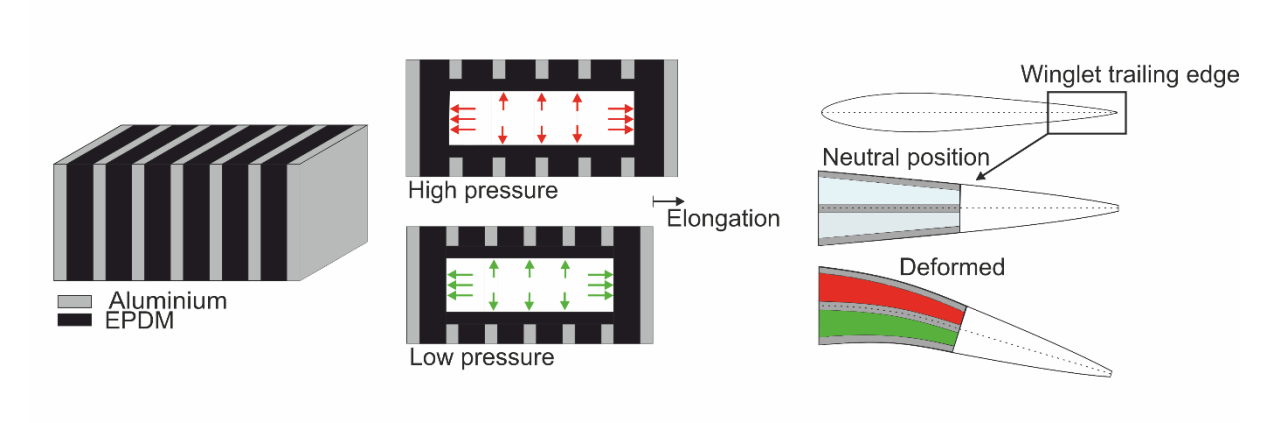


Figure 1 – Functional principle of the pressure cells

This concept can be employed for various functions on the aircraft, including roll (e.g. on ailerons) and variable camber. In the context of this study, a concept for a control surface on a single-aisle aircraft, located at the winglet (referred to as winglet tab), was utilized to enhance flight performance during takeoff, climb, and cruise, as well as to reduce maneuver loads [1]. For performance functionality, deflections between +/- 10° with a deflection rate of 10°/s are required. To achieve maneuver load alleviation, a minimum deflection rate of 20°/s and deflection angles of +/- 15° are needed. From the functional principle and the conducted structural analyses [9], requirements at system level can be derived. It could already be shown in the structural analyses that with the design a maximum deflection of 12° is presumably possible. Table 1 presents the requirements for the winglet tab and the associated actuation system.

Table 1 – Winglet tab requirements on function and system level

Description	Requirement	
Function Level		_
Deflection (performance)	+/- 10°	
Deflection speed (performance)	10°/s	
Deflection (maneuver load alleviation)	+/- 15°	
Deflection speed (maneuver load alleviation)	20°/s	
System Level		
Fluid	gas or liquid	
Maximum fluid pressure	20 bar	
Volume flow (performance)	0.64 l/min	
Volume flow (maneuver load alleviation)	1.28 l/min	

From this concept, a morphing surface demonstrator with the spanwise dimension of one meter has been developed to facilitate integrated system tests [9] (Figure 2). The pressure cell demonstrator is made of aluminum (stiff material) and an Ethylene Propylene Diene Monomer (EPDM) rubber (flexible material). The upper and lower part of the control surface are connected by a Glas-Fibre Reinforced Plastic (GFRP) laminate. In total, the demonstrator has 32 pressure cells (16 on the upper and 16 on the lower side). The structure is divided into passive and active parts. There are two pairs of cells positioned adjacent to each other, with a larger passive region in between (yellow). Each active cell (blue) has an interface for the actuation system and an interface for venting during initialization process (green). Additionally, the structure has interfaces for fiber optic sensors (orange) to determine the deflection angle (see Section 4.1.2).



Figure 2 – Morphing winglet tab demonstrator

In contrast to the design, two significant modifications were made during the manufacturing. These changes were made mainly due to the fact that only one structural demonstrator was available for the experiments, and its damage would have led to the termination of the development. Firstly, the structure has more material in the passive cells compared to the initial design. That is due to resizing in manufacturing after some prototypes exhibiting failure of EPDM while milling. Consequently, the structure withstands a higher maximum pressure but is also stiffer and deforms less under the same pressure. Additionally, an EPDM layer was inserted within the active cells to provide additional safety in case the EPDM detaches from the aluminum. As shown in Figure 3, this results in a reduction of the area within the active cell and thus the effective area of the fluid.

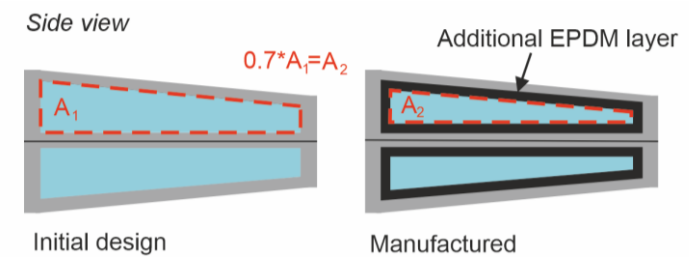


Figure 3 – Differences of the structure of the active cells between initial design and manufacturing

3. System Design

As for the fluid, both air and hydraulics are viable, but investigations in the preliminary design [3] have shown that hydraulic fluid is more suitable for the application. Based on the properties and requirements, a system architecture was designed, aligning with existing certified aircraft actuation systems. In this case, Electro-Hydrostatic Actuators (EHAs) [10] provide the template for the system architecture. The system architecture in connection with the morphing structure is illustrated in Figure 4. The architecture consists of a closed hydraulic circuit driven by an electric motor and a bidirectional pump. The motor controls both the speed and direction, resulting in pump rotation and generation of flow and pressure in the corresponding direction. This, in turn, adjusts the position of the control surface. Whereas EHAs typically use hydraulic cylinders, the present concept directly fills the fluid into the morphing pressure cells. Additionally, valves are integrated, primarily serving system protection from overpressure. Furthermore, components are required to ensure the minimum pressure in the circuit, which can be achieved using either a second pump or an accumulator. In the architecture developed in this work, a pump is used because it enables the initial pressurization of the system at the same time.

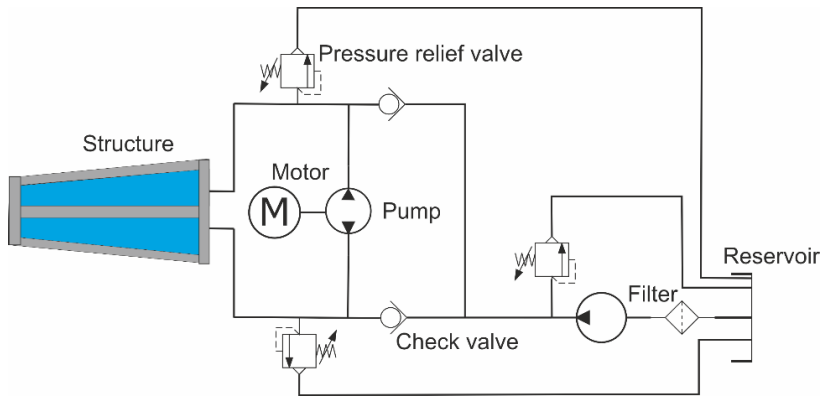


Figure 4 – Actuation system architecture

The control surface is intended to be operated via a closed-loop control system (see Figure 5). The difference between the desired and actual angles is measured, and a speed reference is generated for the motor using a Proportional-Integral (PI) controller. For this type of control, the angle of the control surface must be measured and used as a feedback signal. This can be accomplished using strain gauges or Fiber Bragg Grating (FBG) sensors.

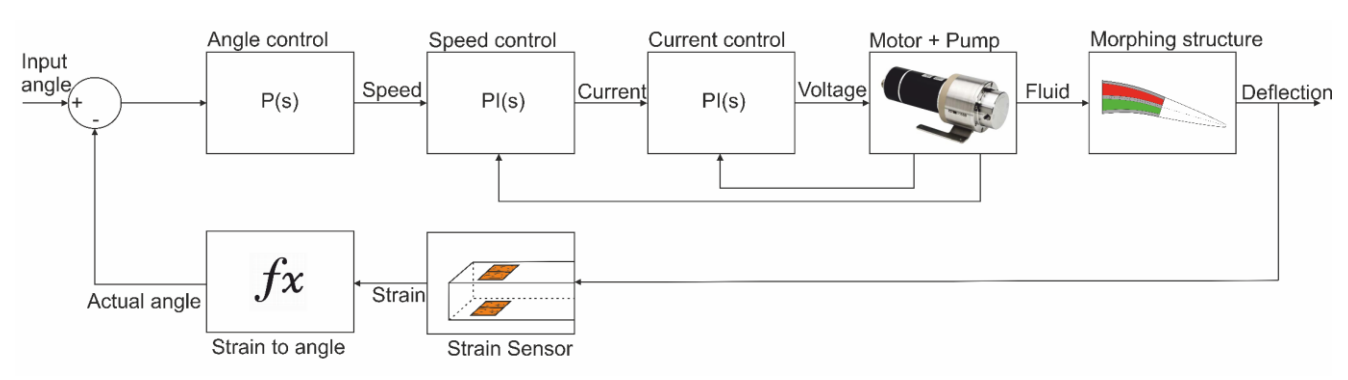


Figure 5 – Closed-loop control system of the morphing winglet tab

4. Testing

Following the design of the system architecture, the functionality of the actuation concept was investigated through simplified simulations [8]. Based on these findings, a test environment with a flight control actuation system prototype was constructed, and a test plan developed. Subsequently, experiments were conducted according to the test plan, and the results were analyzed.

4.1 Test Environment

The test environment for the system can be divided into three subsystems: the main test object, the sensors installed on the test bench, and the control system. These systems will be introduced in the following sections.

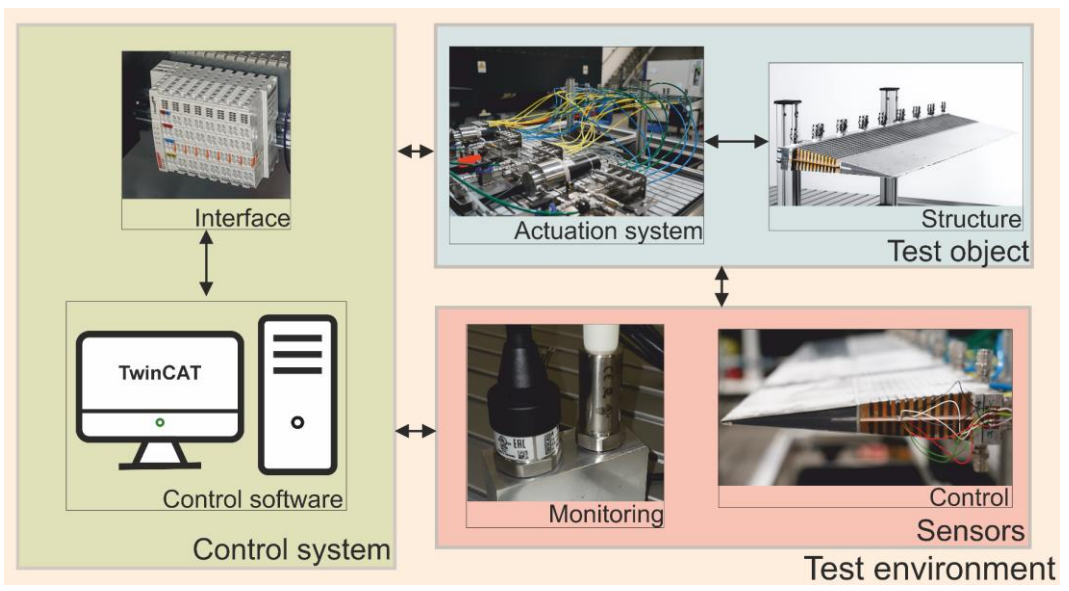


Figure 6 – Test environment for the morphing

4.1.1 Test Object

The general system architecture was described in Chapter 3. For the test setup, an architecture with two parallel-running systems (active/active) was implemented. This redundancy allowed for further investigation beyond simple actuation of the form-variable system, e.g. safety analysis and the consequences of system failure.

Bidirectional gear pumps were chosen for the test bench, driven by BLDC motors. Adjustable relief valves were used for pressure regulation and system safety. Additionally, filters were installed at the pump inlets and outlets to protect the system. All components of the actuation system are made of stainless steel to ensure compatibility with phosphate ester-based fluids commonly used in aviation. Only the connection between the system and the structure was made using PA hoses, facilitating ease of assembly and disassembly during various experiments. It was found, that the use of these hoses has a negligible impact on functionality (e.g. due to hose expansion) compared to stainless steel tubes and could thus be disregarded. The components with their main attribute are summarized in Table 2.

Supply and initialization were carried out using a diaphragm liquid pump. The pump/motor combination, along with check valves and an additional adjustable relief valve, ensured the minimum pressure in the system to protect against cavitation. In addition, the system is equipped with needle valves and venting valves that can be manually opened. These are primarily necessary to purge the system during commissioning. These components are hence not listed in the table, as they do not serve any functionality during the operation of the system.

4.1.2 Sensors

The sensors can be classified into these two categories accordingly. For monitoring purposes, sensors for temperature, pressure, and motor speed measurement are employed. The temperature sensors utilized are Pt100 sensors with a measurement range of 0-100°C. Differential pressure sensors with a measurement range of 0-25 bar are employed for pressure sensing. Motor speed is acquired from the Commercial Off-The-Shelf (COTS) motor controller. To control the system, sensors must be utilized from which the deflection angle of the structure can be determined. A notable challenge arises from the highly nonlinear behavior of the structure (EPDM), necessitating the direct

Table 2 – Installed components on the test rig

Component	Attribute	Value	
Motor	Type	BLDC	
	Power	850 W	
	Torque	4.25 Nm	
	Speed	7600 rpm	
Main pump	Type	Gear pump	
	Deplacement	0.2 ml	
	Max. pressure	60 bar	
	Pressure difference	0-40 bar	
	Speed	6000 rpm	
	Volume flow	0.2-1150 ml/min	
Pressure relief valve (main)	Relief pressure 18 bar (adjus		
	Max. pressure	5.9 bar	
Check valve	Cracking pressure	0.02 bar	

measurement of the control surface deflection angle. In contrast, the deflection angle of classic control surfaces is usually determined by indirect measurement (e.g. actuator stroke).

Two different sensor concepts were installed in the test stand for this purpose. On the one hand, a well-known concept with strain gauge sensors was used. This is widely applied and therefore serves as the baseline for the measurements in the experiments described in this work. On the other hand, an alternative measurement concept is employed with the aid of fiber optic sensors. This approach is not yet widely used in aviation and is therefore considered more experimental. However, Fiber Optic Sensors (FOS) offer several advantages over other measurement methods. These advantages include their ability to be lightweight, very small sized, passive, and immune to ElectroMagnetic Interference (EMI) [11].

The strain gauges were configured in a Wheatstone bridge circuit attached to the deformable structure on the laminate between the two cells. With the supply voltage V_s , the measured output voltage V_0 and the strain gauge specific factor k the strain

$$\varepsilon = \frac{1}{k} \cdot \frac{V_0}{V_S} \tag{1}$$

of the morphing structure can be determined. To determine the surface angle from the strain signal a calibration with an optical image correlation system was performed.

Another method employs FOS measuring the change in light wavelength via FBG. As described in Chapter 2, the demonstrator features four interfaces for the optical fibers. Within each optical fiber, three FBG Sensors with different wavelengths λ_B are embedded. These FBG have different refractive indexes n_2 than the core of the fiber n_1 and hence induce reflection of the light signal. The functionality is illustrated in Figure 7.

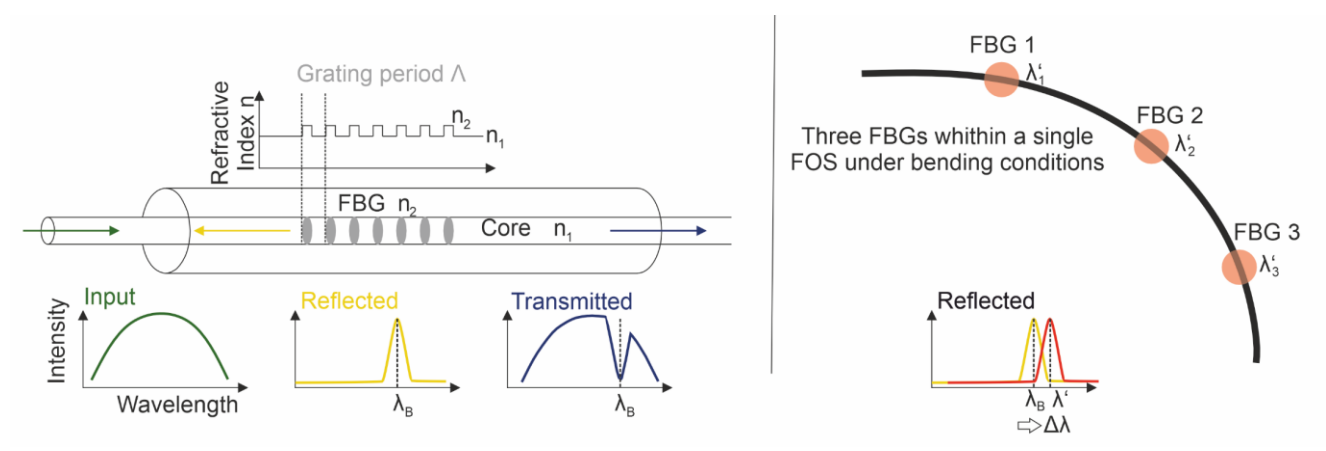


Figure 7 – Functionality of an FBG (right) and FOS under bending conditions (left)

When the optical fiber is bent, the wavelength of the reflected light changes $\Delta\lambda$. From this change, using the strain-optic coefficient p_e , the strain

$$\varepsilon = \frac{\Delta \lambda}{\lambda_B} \cdot \frac{1}{(1 - p_e)} \tag{2}$$

can be determined. Since all experiments take place at room temperature, the temperature influences are neglected in the equation presented here. Since each cable has three FBG sensors, strain can be measured at three positions, allowing for the determination of bending. From this bending profile, the angle can subsequently be determined. Alternatively, calibrations can also be carried out from strain signals as with strain gauge sensors.

4.1.3 Control System

The control of the components and measurement of the systems are carried out using a Programmable Logic Controller (PLC). A *Beckhoff* system is utilized as the PLC, which both reads sensor data and controls the motors of the actuation system. The control of the test bench is accomplished through the programming language Structured Text (ST). In ST, sensor data is recorded, and controllers for the control surface are implemented, enabling hard real-time operation of the test object. In order to protect the test bench from overpressure measures implemented in hardware (pressure relief valve) as well as software (monitoring routines) are utilized.

Since the FOS system used in these tests is equipped only with an USB interface and is hence not real-time capable, reading the signal is done through an indirect method. A driver available in *LabVIEW* is configured accordingly and linked to the PLC system. This allows for control of the outer control-loop using FOS under soft real-time conditions. However, since the outer control-loop requires only a low sampling rate, this limitation is not critical for the experiments presented here. Furthermore, the control of the outer loop can be performed using strain gauges under hard real-time conditions.

4.2 Test Plan

The test plan can be divided into two categories: functional tests and performance tests. For the functional tests, individual structural integrity tests were conducted at maximum pressure, as well as testing the functionality of the system with a simplified setup without a closed-loop control. The performance tests were conducted using the test environment described in Chapter 4.1. Various experiments were carried out for control, dynamic behavior, and fluid performance. The test plan, including the individual experiments and their respective rationales, is depicted in Table 3. In this paper, the focus lies on the performance tests.

Table 3 – Test plan

No	Тур	Test	Rational
1	Functional		
1.1		Maximum pressure	 Structural Integrity
		System design	 Initialization of the system
1.2			 Actuation of the system in both directions
2	Performance		
		Closed-loop control	 Controller tuning
2.1			 Maximum performance (speed and angular displacement)
			Angle accuracy
2.2		Dynamic behavior	Bode diagram
			Gain and phase lag
2.3		Fluid performance	 Influence of fluid viscosity on performance (water vs. hydraulic oil)

4.3 Performance Test Results

4.3.1 Closed-Loop control

At the beginning of the test procedure, the control loop parameters had to be defined. Initially, the parameters of the two inner motor control loops (current and speed) were determined using the motor parameters and *Matlab* software. Subsequently, the outer position control loop was. It is crucial to note that overshooting is generally undesirable in position control of control surfaces. The control loop is thus only allowed to overshoot within the range of control accuracy for controller adjustment. The parameter of the control loop was adjusted based on experiments conducted at the test stand.

Table 4 – Closed-loop control parameter

Position control	Speed control		ion control Speed control Current control		control
P [U/min/°]	P [As]	l [µs]	P [mOhm]	l [µs]	
2000	1,5328	909	800	650	

During the experiments, a force fight between the two actuation systems was identified. The occurrence of such a force fight was expected, as it also occurs in classical active/active actuation of control surfaces. The force fight can have various causes, with manufacturing tolerances of the system and its structure playing a crucial role. In the system under consideration, the force fight manifests as a pressure difference between the two parallel systems. As a result, one system is always subjected to higher stress than the other. Therefore, a force fight during operation is undesirable.

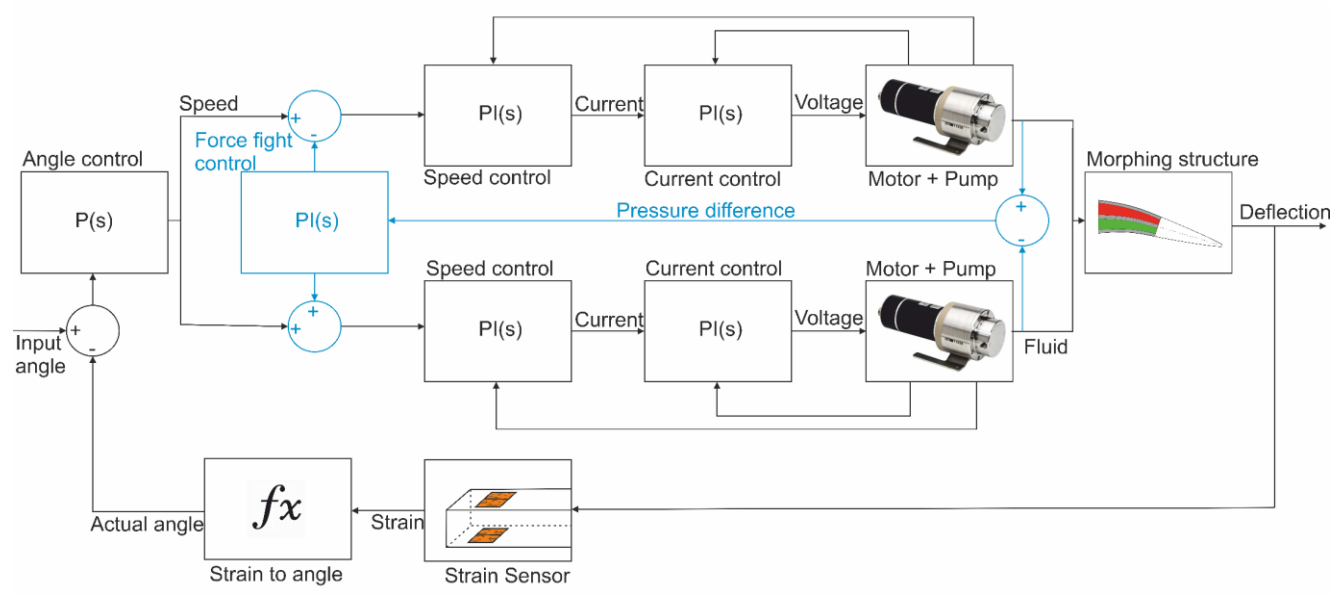


Figure 8 – Closed-loop control system with force fight controller in active/active mode

To minimize this effect, an additional PI controller is implemented (blue in Figure 8). The pressure difference is determined from the pressure sensors and serves as input for the force fight control. The PI controller outputs a speed correction within a restricted range (2% of the maximum pump speed). This speed is added to the speed setpoint of one system and subtracted from the other system. Thus, both systems receive a slightly modified speed setpoint.

The pressure signal profile during actuation with and without the force fight controller is illustrated in Figure 9. While actuation without the force fight controller results in a pressure difference of 2.5 bar between both systems, the pressure difference reduces to nearly 0 bar during actuation with the force fight controller active.

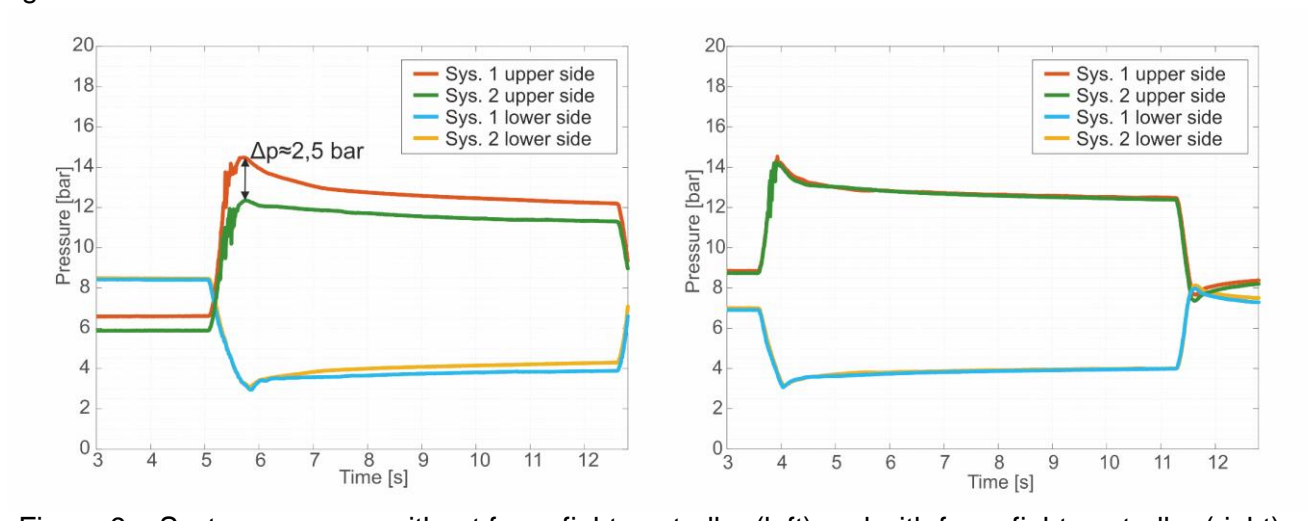


Figure 9 – System pressure without force fight controller (left) and with force fight controller (right)

After the implementation of the control loops, experiments on the system behavior were conducted. At the beginning of the test series, maximum possible deflection angles, deflection rates, and position accuracy were investigated. Figure 10 illustrates the step response of the system with the controller parameters depicted above. Here, the step signal corresponds to a deflection of 4°. A maximum actuation velocity of approximately 11.8 °/s is achieved. The deflection shows a slight overshoot, but it is still within the allowed range of control accuracy (green area).

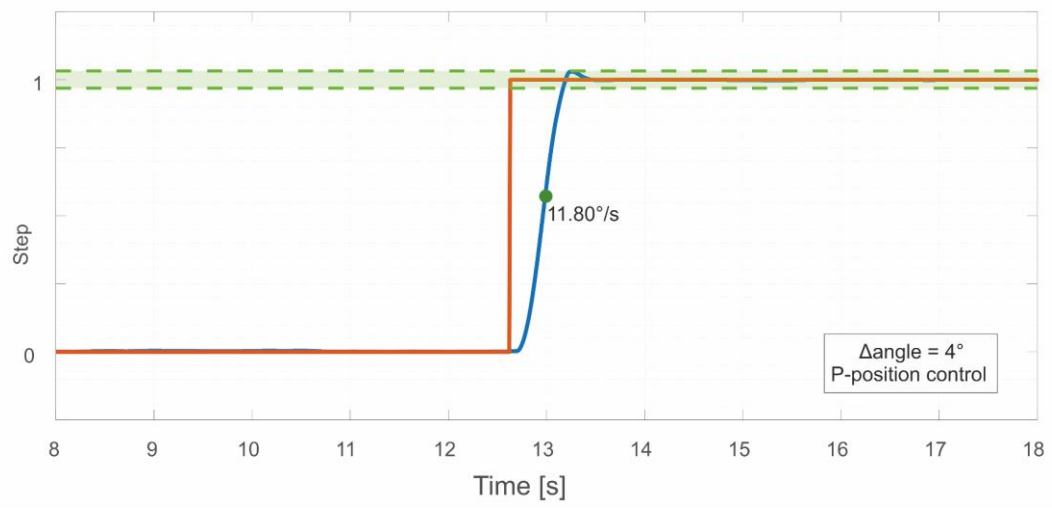


Figure 10 – Step response of the system

In Figure 11 images of the structure from the side are shown, once in the neutral state (left) and with a deformation of a 5° deflection angle (right).



Figure 11 – Morphing structure deflection test: neutral position (left) and 5° deflection (right)

In comparison to the requirements described in Table 1, it must be noted that the speed of the system only meets the requirement for maneuverability, but not for load alleviation. Similarly, the maximum achievable angle with a pressure difference of 15 bar is not as designed at 12° [9] but approximately 5°. These two observations can likely be attributed to the changes of the design during the manufacturing of the structure described in Chapter 2. Taken together, these changes lead to a significantly stiffer structure with a smaller effective area for the fluid. Therefore, it can be assumed that the performance of the entire system is reduced due to these measures. If these design changes are included in a first rough calculation of the structure model, the results match by 95%. However, further detailed investigations are necessary to confirm the results.

4.3.2 Dynamic Behavior

Dynamic experiments for system identification were conducted, utilizing sinusoidal signals as position input for the control surface with varying amplitudes and periods. From these experiments, the amplitude gain and phase lag were determined.

For the analysis of dynamic behavior, the system was subjected to sinusoidal signals with progressively increasing frequencies while maintaining constant amplitude as input. These experiments were performed within a closed-loop control system, where both the maximum deflection speed and the phase lag, along with the gain, were determined. Figure 12 depicts the response for a frequency of 0.5 Hz with amplitudes of 0.5° and 3°. The gain for experiments measured at a frequency of 0.5 Hz was -0.25 dB for an amplitude of 0.5° and -0.1 dB for an amplitude of 3°. The phase lag observed in the presented experiments were -27.0° and -23.4°, respectively.

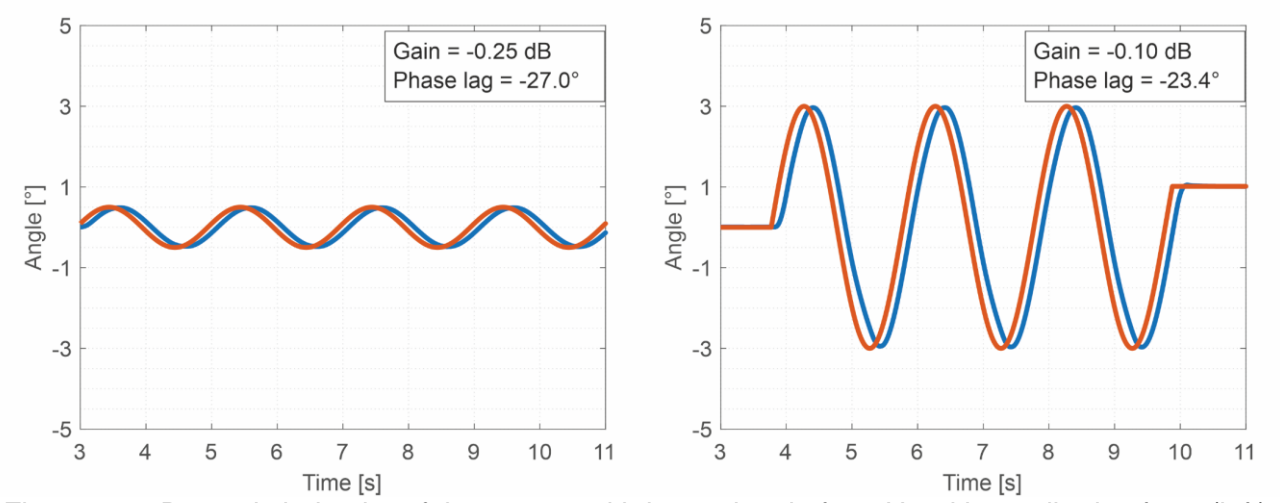


Figure 12 – Dynamic behavior of the system with input signal of 0.5 Hz with amplitude of 0.5°(left) and 3°(right)

Subsequently, the frequency was varied for further experiments. From the results, the bode diagrams for the closed-loop control system were derived for the different amplitudes. The bode diagrams for an amplitude of 0.5° are depicted in Figure 13. These data points were fitted using regression with a third-degree polynomial. The quality of fit, indicated by the R-squared value of 0.996 and 0.994, respectively, demonstrates a high level of consistency with the measured data points.

4.3.3 Fluid Performance

The chosen fluid significantly influences the operation of the entire system, with compressibility and viscosity playing crucial roles. In the aerospace domain, only specific fluids meeting requirements for temperature ranges and flammability [12] are permitted. While gases exhibit compressibility, liquids have low compressibility and can often be simplified as incompressible in low-pressure conditions. From investigations within the preliminary design [3], it was concluded that the use of a liquid is advantageous over a gas. Accordingly, only liquids are employed in the experimental setup. The most significant difference in using liquids arises from viscosity. To examine properties, two liquids with vastly different viscosities were used: water with a viscosity of 1 mm²/s at room temperature and a water-based hydraulic oil with a viscosity of about 140 mm²/s at room temperature.

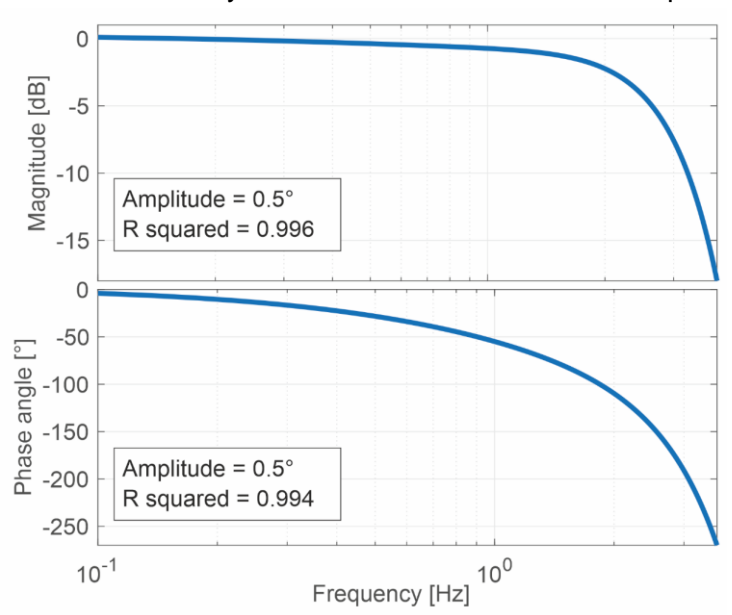


Figure 13 – Bode plot for a sinusoidal signal with amplitude of 0.5°

Figure 14 illustrates the step response of the system using water. It is evident from the figures that with water, the proportional control of position is sufficient to attain the desired angle. However, achieving the desired angle requires the addition of an integral component in the control-loop. As shown in Section 4.3.1, an integral component is unnecessary when using hydraulic oil. Incorporating

an integral component in position control has the disadvantage of slowing down the system's response. Additionally, an excessively high integral component can lead to unstable system behavior.

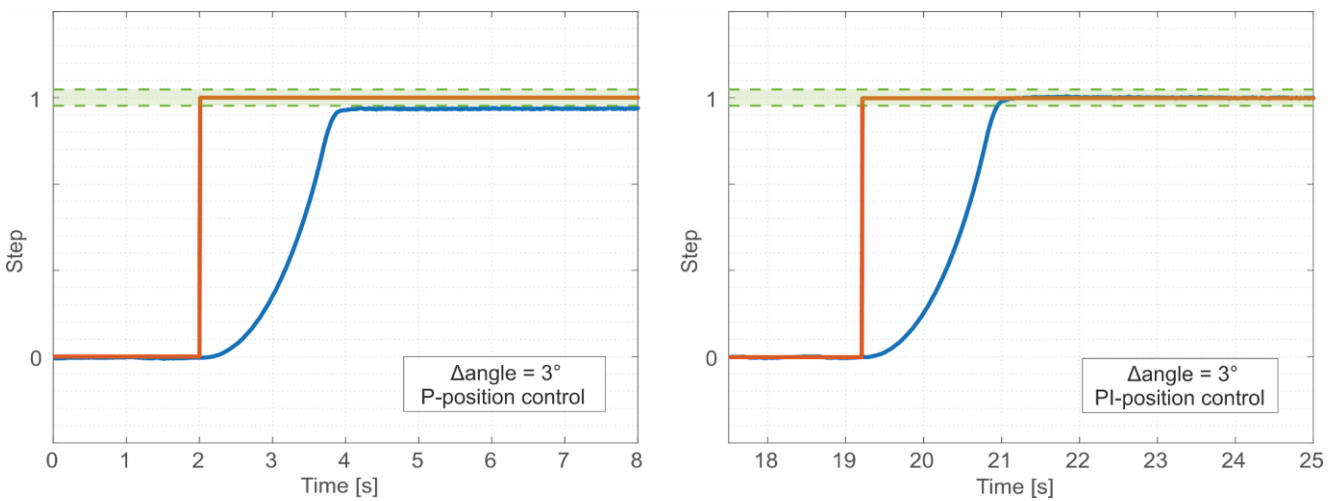


Figure 14 – Step response using water without (left) and with (right) integral controller component

Figure 15 illustrates the differences between water and oil regarding the force fight of the two systems. To measure this, the integrated force fight control-loop from Section 4.3.1 was deactivated. The force fight is visible based on the pressure within the two systems. A significant contrast between the two fluids is observable. The force fight in the system with water is notably higher and amplifies continuously while maintaining a position. Small discrepancies in the system thus have a much more pronounced effect with low viscosity fluid compared to a fluid with high viscosity.

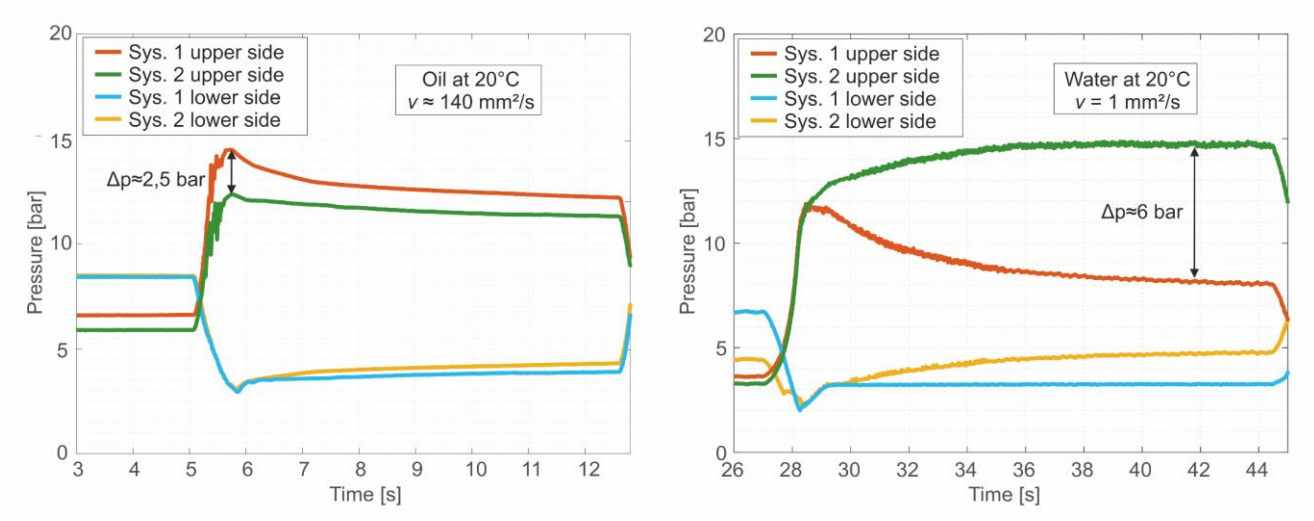


Figure 15 – Force fight behavior of the system using oil (left) and water (right)

The results indicate that the behavior of the hydraulic oil surpasses water in the depicted aspects due to its higher viscosity. However, a drawback of higher viscosity is an increased power requirement of the system. Nonetheless, the advantages outweigh the disadvantages in the system under consideration. Based on these findings, further investigations can explore various viscosities to determine the optimal behavior.

5. Conclusion

In this work, an actuation system for a novel morphing technology was developed and its functionality was demonstrated through experiments. In addition to pure performance investigations, further aspects were analyzed using the test setup. The dynamic behavior was examined in various frequency ranges, as well as the effects of fluids with different viscosities on the overall system. The fundamental functionality was proven with these experiments. However, the performance is lower than initially anticipated, which can be attributed to various factors. Additional safety features added during manufacturing are likely the main contributing factor. Furthermore, the investigations revealed the presence of a force fight in the system, which can be minimized with an additional control-loop.

In the next steps, a detailed dynamic model of the test setup will be developed. The results from simulations will be compared with experimental findings. Subsequently, a detailed design of the overall system will be carried out based on the model, aiming to achieve performance optimization.

A crucial step from a structural perspective is the development of manufacturing processes for such types of structures. The demonstrator tested here is a custom-made product that could only be manufactured with considerable effort. Similarly, efforts are underway to reduce the system's size. There is significant potential here, as the functional demonstration relied solely on COTS components, allowing flexibility in architectural changes. Since the experiments have shown that the functionality of the concept, specific components with significantly reduced size can be purchased and/or developed.

6. Contact Author Email Address

michael.schaefer@dlr.de

7. Acknowledgments

This project has received funding from Clean Sky 2 Joint Undertaking under the European Union's Horizon 2020 research and innovation programme under grant agreement No CS2-Air-GAM-20142015-01.

8. Copyright Statement

The authors confirm that they, and their company, hold copyright on all of the original material included in this paper. The authors also confirm that they have obtained permission, from the copyright holder of any third-party material included in this paper, to publish it as part of their paper. The authors confirm that they give permission, or have obtained permission from the copyright holder of this paper, for the publication and distribution of this paper as part of the ICAS proceedings or as individual off-prints from the proceedings.

References

- [1] Bolonkin A. Estimated Benefits of Variable-Geometry Wing Camber Control for Transport Aircraft, NASA Report, 1999.
- [2] Vasista S and Tong L. Design Considerations of a Pressure Driven Morphing Wing Structure, in *Proceedings of the 28th Congress of the International Council of the Aeronautical Sciences*, Brisbane, Australia, September 23 28, 2012.
- [3] Schäfer M, Schäfer A and Bertram O. Preliminary Design of Hydraulic and Pneumatic System Architectures for a Morphing Flight Control Structure, *SAE Technical Paper*, 2019.
- [4] Van Eemeren A. Joint Development for a Morphing Wing Skin, Delft, Netherlands: Delft University of Technology, 2021.
- [5] Barbarino S, Ameduri S, Lecce L and Concilio A. Wing Shape Control through an SMA-Based Device, Journal of Intelligent Material Systems and Structures, 2009.
- [6] Lee T and Chopra I. Design of piezostack-driven trailing-edge flap actuator for helicopter rotors, *Smart Materials and Structures*, Vol. 10, pp. 15, 2001.
- [7] Vasista S and Tong L. Topology-optimized design and testing of a pressure-driven morphing-aerofoil trailing-edge structure, *AIAA journal, Vol.* 51, pp. 1898–1907, 2013.
- [8] Schäfer M, Bertram O, Vasista S and Seer D. Systementwicklung für eine formvariable Struktur an der Flügelhinterkante, in *Smarte Strukturen und Systeme Tagungsband des 4SMARTS-Symposiums*, 2022.
- [9] Vasista S, Nolte F, Schäfer M and Riemenschneider J. Design and Manufacture of a Fluid-Actuated Morphing Winglet Trailing Edge Control Surface, in *ASME 2022 Conference on Smart Materials, Adaptive Structures and Intelligent Systems*, Michigan, USA, September 12 14, 2022.
- [10] Alle N, Hiremath S, Makaram S, Subramaniam K and Talukdar A. Review on electro hydrostatic actuator for flight control, *International Journal of Fluid Power, Vol.* 17, pp. 125–145, 2016.
- [11] Campanella C, Cuccovillo A, Campanella C, Yurt A und Passaro V. Fibre Bragg Grating Based Strain Sensors: Review of Technology and Applications, *Sensors*, Vol. 18, p. 3115, 2018.
- [12] SAE International. Fire Resistant Phosphate Ester Hydraulic Fluid for Aircraft AS1241D, SAE Standard, 2016.